

## RESEARCH ARTICLE

# Distinct intracellular $\text{Ca}^{2+}$ dynamics regulate apical constriction and differentially contribute to neural tube closure

Makoto Suzuki<sup>1,2,¶</sup>, Masanao Sato<sup>2,3,4,\*</sup>, Hiroshi Koyama<sup>2,5,§</sup>, Yusuke Hara<sup>1,2,†</sup>, Kentaro Hayashi<sup>1,2</sup>, Naoko Yasue<sup>1</sup>, Hiromi Imamura<sup>6</sup>, Toshihiko Fujimori<sup>2,5</sup>, Takeharu Nagai<sup>7</sup>, Robert E. Campbell<sup>8</sup> and Naoto Ueno<sup>1,2,¶</sup>

## ABSTRACT

Early in the development of the central nervous system, progenitor cells undergo a shape change, called apical constriction, that triggers the neural plate to form a tubular structure. How apical constriction in the neural plate is controlled and how it contributes to tissue morphogenesis are not fully understood. In this study, we show that intracellular calcium ions ( $\text{Ca}^{2+}$ ) are required for *Xenopus* neural tube formation and that there are two types of  $\text{Ca}^{2+}$ -concentration changes, a single-cell and a multicellular wave-like fluctuation, in the developing neural plate. Quantitative imaging analyses revealed that transient increases in  $\text{Ca}^{2+}$  concentration induced cortical F-actin remodeling, apical constriction and accelerations of the closing movement of the neural plate. We also show that extracellular ATP and N-cadherin (*cdh2*) participate in the  $\text{Ca}^{2+}$ -induced apical constriction. Furthermore, our mathematical model suggests that the effect of  $\text{Ca}^{2+}$  fluctuations on tissue morphogenesis is independent of fluctuation frequency and that fluctuations affecting individual cells are more efficient than those at the multicellular level. We propose that distinct  $\text{Ca}^{2+}$  signaling patterns differentially modulate apical constriction for efficient epithelial folding and that this mechanism has a broad range of physiological outcomes.

**KEY WORDS:** Actomyosin, Apical constriction,  $\text{Ca}^{2+}$ , Epithelial remodeling, Neural tube closure

## INTRODUCTION

The construction of multicellular biological systems requires substantial tissue movement based on the collective motility of single cells. Problems such as congenital malformations,

breakdown of homeostasis and cancer can arise when the mechanisms that guide the concerted movement of single cells are dysfunctional (Guillot and Lecuit, 2013). In vertebrates, the central nervous system (CNS) is established during early embryogenesis by the collective closing movement of an epithelial sheet of neural progenitor cells in a process called neural tube closure (NTC), and NTC failure causes a common human birth defect (Copp et al., 2003; Suzuki et al., 2012). During NTC, neuroepithelial cells on the dorsal side contract and stabilize their apical sides to change from a columnar to a wedge shape. As a common strategy for folding an epithelial sheet, this cellular morphogenesis, called apical constriction (AC), generates physical force to bend the neural plate (NP) inward (Martin and Goldstein, 2014; Sawyer et al., 2010; Suzuki et al., 2012). The lateral edges of the bending neural plate lift above the dorsal surface, eventually come together along the dorsal midline and fuse to form the neural tube.

AC involves the accumulation of actin filaments (F-actin) at the apical side, where non-muscle myosin II generates contractile force. Thus, AC is thought to be controlled by a coordinated action of cytoskeletal networks, cell-cell adhesions and their regulators (Martin and Goldstein, 2014; Sawyer et al., 2010; Suzuki et al., 2012). However, how AC in the individual cell is controlled collectively within the tissue and how AC contributes to tissue remodeling are not fully understood. Recent studies have revealed that the AC in *Drosophila* and *Caenorhabditis elegans* epithelial invaginations is highly dynamic and is governed by oscillations of the apical actomyosin network, in which cell contraction is followed by stabilization (Martin and Goldstein, 2014; Mason et al., 2013; Sawyer et al., 2010). Hence, we hypothesized that the signaling pathway that induces rapid cellular behaviors controls AC during NTC.

In this study, we examined the roles of intracellular calcium ion ( $\text{Ca}^{2+}$ ) signaling in NTC. Generally, the intracellular  $\text{Ca}^{2+}$  concentration is maintained at a low level under basal conditions and is transiently increased by  $\text{Ca}^{2+}$  influx through membrane-localized  $\text{Ca}^{2+}$  channels or release from the endoplasmic reticulum via channels such as the inositol triphosphate receptor ( $\text{IP}_3\text{R}$ ) (Clapham, 2007).  $\text{Ca}^{2+}$  binds to and activates its target proteins that control diverse biological phenomena, such as cell proliferation, muscle contraction, gene expression and cellular movement (Clapham, 2007; Markova and Lenne, 2012). Inhibiting  $\text{Ca}^{2+}$  influx causes NTC to fail (Lee and Nagele, 1986; Smedley and Stanisstreet, 1986), while inducing an increase in intracellular  $\text{Ca}^{2+}$  promotes folding morphogenesis of the NP (Ferreira and Hilfer, 1993; Moran and Rice, 1976). Since these effects at the tissue level are accompanied by changes in cell shape (Ferreira and Hilfer, 1993), intracellular  $\text{Ca}^{2+}$  signaling has been proposed to regulate AC, although the detailed molecular mechanism is unclear.

<sup>1</sup>Division of Morphogenesis, National Institute for Basic Biology, National Institutes of Natural Sciences, Okazaki, Aichi 444-8585, Japan. <sup>2</sup>Department of Basic Biology, School of Life Science, the Graduate University of Advanced Studies, Hayama, Kanagawa 240-0193 Japan. <sup>3</sup>Division of Developmental Genetics, National Institute for Basic Biology, National Institutes of Natural Sciences, Okazaki, Aichi 444-8787, Japan. <sup>4</sup>Department of Biodesign Research, Okazaki Institute for Integrative Bioscience, National Institute for Basic Biology, National Institutes of Natural Sciences, Okazaki, Aichi 444-8787, Japan. <sup>5</sup>Division of Embryology, National Institute for Basic Biology, National Institutes of Natural Sciences, Okazaki, Aichi 444-8787, Japan. <sup>6</sup>Department of Functional Biology, Graduate School of Biostudies, Kyoto University, Sakyo-ku, Kyoto 606-8501, Japan. <sup>7</sup>Department of Biomolecular Science and Engineering, The Institute of Scientific and Industrial Research, Osaka University, Ibaraki, Osaka 567-0047, Japan. <sup>8</sup>Department of Chemistry, University of Alberta, Edmonton, Alberta, Canada T6G 2G2.

\*Present address: Division of Applied Bioscience, Graduate School of Agriculture, Hokkaido University, Sapporo, Hokkaido 060-8589, Japan. †Present address: Mechanobiology Institute, National University of Singapore, 117411 Singapore.

§These authors contributed equally to this work

¶Authors for correspondence (msuzuki@nibb.ac.jp; nueno@nibb.ac.jp)

© M.S., 0000-0002-5494-6593

## RESULTS

Physiological significance of intracellular  $\text{Ca}^{2+}$  in NTC

We first examined the role of intracellular  $\text{Ca}^{2+}$  signaling during NTC in the African clawed frog, *Xenopus laevis* (Fig. S1) by using pharmacological treatments. Perturbing the  $\text{Ca}^{2+}$  influx with 2-aminoethoxydiphenyl borate (2APB, which blocks  $\text{IP}_3\text{R}$  and other membrane-localized  $\text{Ca}^{2+}$  channels) or with nifedipine (which blocks voltage-dependent  $\text{Ca}^{2+}$  channels) inhibited NTC (Fig. 1A). We confirmed these results by measuring the width of NP using expression of the pan-neural marker *Sox2* (Fig. 1B). Phalloidin staining revealed that AC in NP cells was inhibited, thus delaying folding morphogenesis of the NP (Fig. 1C,D). Since these inhibitors did not change the expression patterns of marker genes (Fig. 1E), these results suggest that  $\text{Ca}^{2+}$  signaling regulates AC during NTC independently of neural development.

Live-imaging analyses of  $\text{Ca}^{2+}$  fluctuation

In a number of organisms, including *Xenopus*, active changes of intracellular  $\text{Ca}^{2+}$  concentration have been observed during development (Hunter et al., 2014; Leclerc et al., 2000; Markova and Lenne, 2012; Shindo et al., 2010; Wallingford et al., 2001). Therefore, we hypothesized that  $\text{Ca}^{2+}$  signaling is spatially and temporally correlated with cellular morphogenesis. We investigated the patterns of intracellular  $\text{Ca}^{2+}$  concentration changes during NTC using live cell-imaging analyses with transiently expressed genetically encoded  $\text{Ca}^{2+}$  indicators for optical imaging (GECOs) (Fig. S2A) (Zhao et al., 2011). The intensity of R-GECO1.0 fluorescence fluctuated actively throughout the NP at both single-cell and whole-tissue levels (Fig. 2; Movie 1). In this study, we defined a single increase and the following decrease in GECO fluorescence intensity as a  $\text{Ca}^{2+}$  ‘transient’. We

observed two spatial patterns of  $\text{Ca}^{2+}$  transients, one that occurred at the single-cell level and lasted less than 40 s (Fig. 2A,C) and another that originated from one or a few cells and propagated radially, wave-like, across neighboring cells until anywhere from several cells to hundreds of cells were involved (Fig. 2B; Movie 2). These multicellular  $\text{Ca}^{2+}$  fluctuations lasted up to 100 s (Fig. 2C). The fold changes in fluorescence intensity were larger at the multicellular level than those at the single-cell level (Fig. 2C). The multicellular waves spread at a speed of  $3.3 \pm 0.94 \mu\text{m/s}$  (mean  $\pm$  s.d.), and larger waves spread at higher speeds (Pearson’s  $r=0.499$ ,  $P=0.0213$ , Fig. 2D), suggesting that a relationship between the wave propagation and the spatial strength of the  $\text{Ca}^{2+}$  signaling contributes to diverse patterns of the  $\text{Ca}^{2+}$  fluctuation.

Quantitative analyses of the  $\text{Ca}^{2+}$  fluctuation

To characterize the spatial and temporal patterns of these  $\text{Ca}^{2+}$  fluctuations more precisely, we conducted quantitative image analyses based on ratiometric imaging (Fig. S2B; Materials and Methods). After extracting and visualizing the  $\text{Ca}^{2+}$  fluctuation profiles, we confirmed that most of the  $\text{Ca}^{2+}$  transients occurred in the NP rather than in the non-neural ectoderm (Christodoulou and Skourides, 2015), which is lateral to the NP and did not undergo folding morphogenesis (Fig. 3A). We quantified the number of  $\text{Ca}^{2+}$  transients as a function of time and found that the number of single-cell transients particularly increased in the last 100 min before NTC was completed (Fig. 3B,C; Fig. S3A). Therefore, we divided the NTC process into an early and a late phase (Fig. 3B). The number of multicellular transients was one order of magnitude smaller than that of single-cell transients throughout the NTC process, and the number of transients remained constant through both the early and

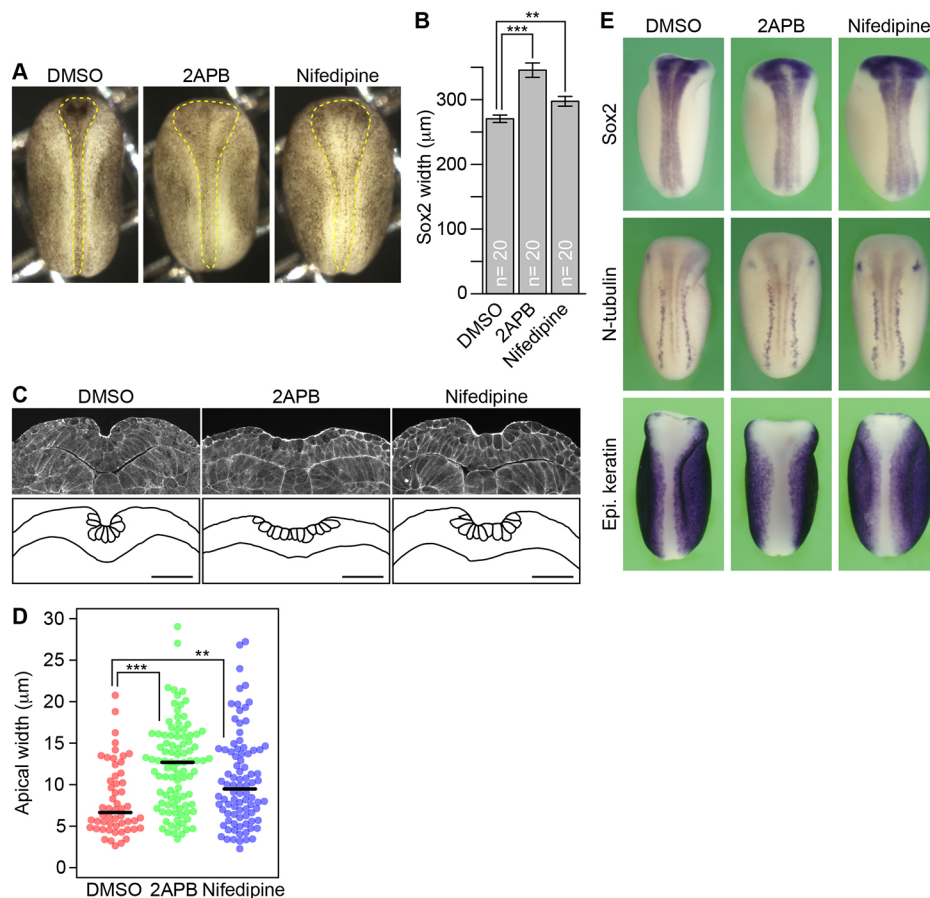


**Fig. 1. Intracellular  $\text{Ca}^{2+}$  is required for *Xenopus* NTC.** (A) Dorsal views of embryos at stage 16 treated with DMSO, 25  $\mu\text{M}$  2APB and 200  $\mu\text{M}$  nifedipine. Dashed lines indicate the outlines of the NP. (B) The mean width of the NP in embryos, as measured by visualizing the expression of the pan-neural marker gene *Sox2*. Error bars depict s.e.m. The number of embryos examined is shown on each bar.  $**P<0.01$  and  $***P<0.001$  compared with the DMSO-treated control; two-sided Welch’s *t*-test. (C) Transverse sections of stage-16 embryos stained with phalloidin (top) and outlines of neural tissues and cells (bottom). Scale bars: 100  $\mu\text{m}$ . (D) Apical width of stage-16 embryos. Black line indicates the median value.  $**P<0.01$  and  $***P<0.001$ , two-sided Mann–Whitney *U*-test;  $n=54$  cells, nine embryos (DMSO); 97 cells, 12 embryos (2APB); 88 cells, 12 embryos (nifedipine). (E) *In situ* hybridization analysis of inhibitor-treated embryos. Dorsal views showing the expression of *Sox2*, a pan-neural marker (top), *N-tubulin* (*tubb2b*), which marks differentiated neurons (middle), and *Epidermal keratin* (Epi. keratin), an epidermal marker (bottom). Anterior is to the top. The expression patterns were similar in inhibitor-treated embryos and DMSO-treated controls, but the expression domains were wider in the inhibitor-treated embryos because of delayed NTC.

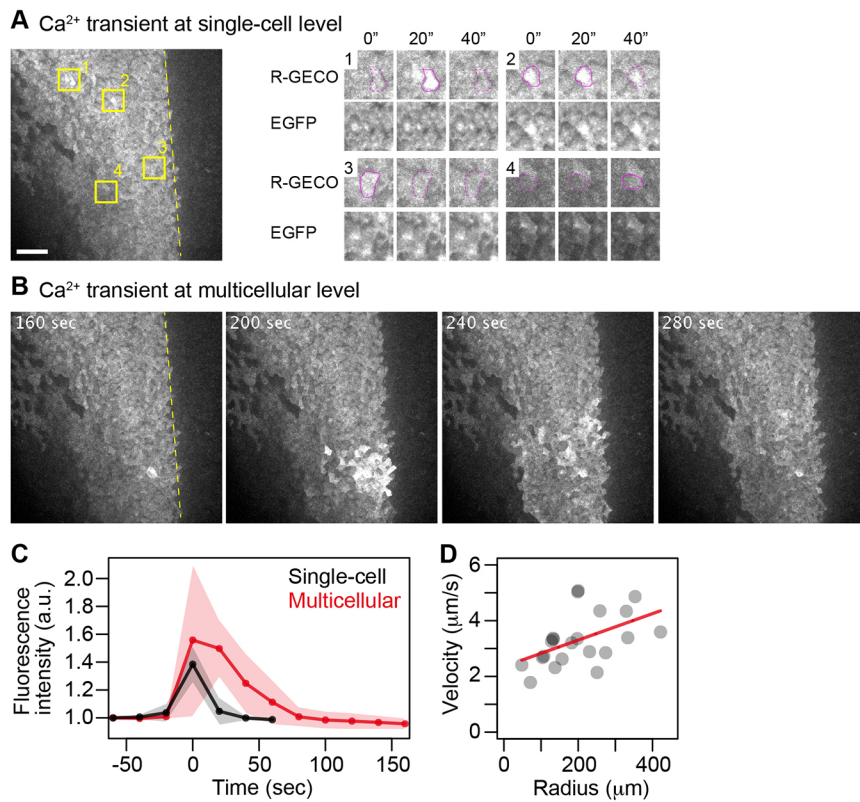


**Fig. 2. Live-imaging analyses of intracellular Ca<sup>2+</sup> in the neural plate.** (A) A Ca<sup>2+</sup> transient at the single-cell level, visualized with R-GECO1.0 (gray), in a dorsal view of the presumptive anterior spinal cord region; anterior is to the top. R-GECO1.0 was introduced on the left side of the embryo. The midline is indicated by a dotted line. A time course over a 40 s period of four sample cells (which are indicated in the figure) is shown in the right panels. Scale bar: 100 μm. (B) Time-lapse imaging data of a multicellular, wave-like Ca<sup>2+</sup> transient in the embryo shown in A. (C) Fluorescence intensities of cytoplasmic R-GECO1.0 over time; the shaded area indicates the s.d. In multicellular Ca<sup>2+</sup> transients (red), cells adjacent to the cell that was initially activated were measured ( $n=6$  cells). (D) The radius and velocity of wave propagations in multicellular Ca<sup>2+</sup> transients. The red line represents the relationship between the two data sets, calculated using the least-squares method of linear regression ( $n=21$  cells, five embryos).

late phases (Fig. 3D). Taken together, these results suggest that single-cell Ca<sup>2+</sup> transients were more frequent in the late phase than in the early phase, whereas the spatial scale (the propagative property) of the Ca<sup>2+</sup> transients was larger in the early phase than in the late phase. The technical limitations of our method did not allow us to segment individual cell outlines, so we could not compare the total number of cells contributing to the Ca<sup>2+</sup> transients. Therefore, we determined the total area of each type of transient and confirmed that the ratio value of the multicellular transients to the single-cell transients decreased from 0.55 to 0.18 in the late phase of NTC (Fig. 3E). These results suggest that the effect of Ca<sup>2+</sup> fluctuations on NTC was derived from both single-cell and multicellular transients in the early phase, but mostly from single-cell transients in the late phase.

### Ca<sup>2+</sup> fluctuation precedes NTC

In our observations, the multicellular wave-like Ca<sup>2+</sup> propagations were associated with a slight deformation of the neural plate tissue (Movies 1 and 2). Together with the observations that perturbation of Ca<sup>2+</sup> influx inhibits NTC, it is suggested that intracellular Ca<sup>2+</sup> signaling is essential for the movements that close the neural tube. We compared the temporal pattern of NTC movements with the total intensity values of R-GECO1.0 at tissue level. As expected, peaks in the R-GECO1.0 temporal profile overlapped with peaks in the speed of the closing movements, both in the early and late phase (Fig. 3F). Cross-correlation analyses revealed a maximum correlation when the R-GECO1.0 value was shifted 20 s later in time (Fig. 3G). Thus, the Ca<sup>2+</sup> fluctuation slightly and consistently preceded the tissue movements to close the neural tube.

### Regulatory mechanisms upstream of the Ca<sup>2+</sup> fluctuation

We examined the effect of the pharmacological treatment on Ca<sup>2+</sup> fluctuations. 2APB suppressed both the single-cell and multicellular

transients in the early phase, whereas nifedipine did not clearly exhibit suppression effects on the multicellular transients (Fig. 3A-D; Fig. S3A). These results suggest that the IP<sub>3</sub>R pathway regulates both types of Ca<sup>2+</sup> transient, whereas the voltage-dependent Ca<sup>2+</sup> channel preferentially regulates Ca<sup>2+</sup> transients at the single-cell level. Cross-correlation analyses revealed that 2APB completely abolished the temporal correlation between Ca<sup>2+</sup> fluctuations and movements of the NP toward closing the neural tube compared with nifedipine (Fig. 3G). This difference might be due to residual multicellular transients in the nifedipine-treated embryo that induced a transient acceleration in the closing movement of the NP (Fig. 3D). Treatment with 2APB or nifedipine did not affect the basal intracellular Ca<sup>2+</sup> level, as estimated using the ultrasensitive Ca<sup>2+</sup> indicator yellow Cameleon-Nano (YC-Nano) (Horikawa et al., 2010) (Fig. S3B). This result suggests that, at the concentrations used, these inhibitors selectively affected the active Ca<sup>2+</sup> fluctuations, and therefore, that the active Ca<sup>2+</sup> signaling is required for NTC.

During *Xenopus* gastrulation, a purinergic receptor (Corriden and Insel, 2010; Schwiebert and Zsembery, 2003) for extracellular ATP (eATP) is required for frequent Ca<sup>2+</sup> elevations (Shindo et al., 2010; Wallingford et al., 2001), and early ectodermal cells respond to eATP causing transient contractions of their apical side (Kim et al., 2014). To examine the possibility that eATP is involved in Ca<sup>2+</sup> fluctuations in the NP, we exhausted the eATP by overexpressing *Xenopus* ectonucleoside triphosphate diphosphohydrolase 1 (E-NTPDase1) (Massé et al., 2007). E-NTPDase1 decreased the frequency of both single-cell and multicellular Ca<sup>2+</sup> transients compared to an enzymatically inactive variant of E-NTPDase1 ( $\Delta$ ACR) (Fig. 4A-C; Fig. S3C, Movie 3). Moreover, overexpressing E-NTPDase1 abolished the temporal correlation between Ca<sup>2+</sup> fluctuations and the closing movements of the NP, as seen with the 2APB treatment (Fig. 4D). We further examined the involvement of

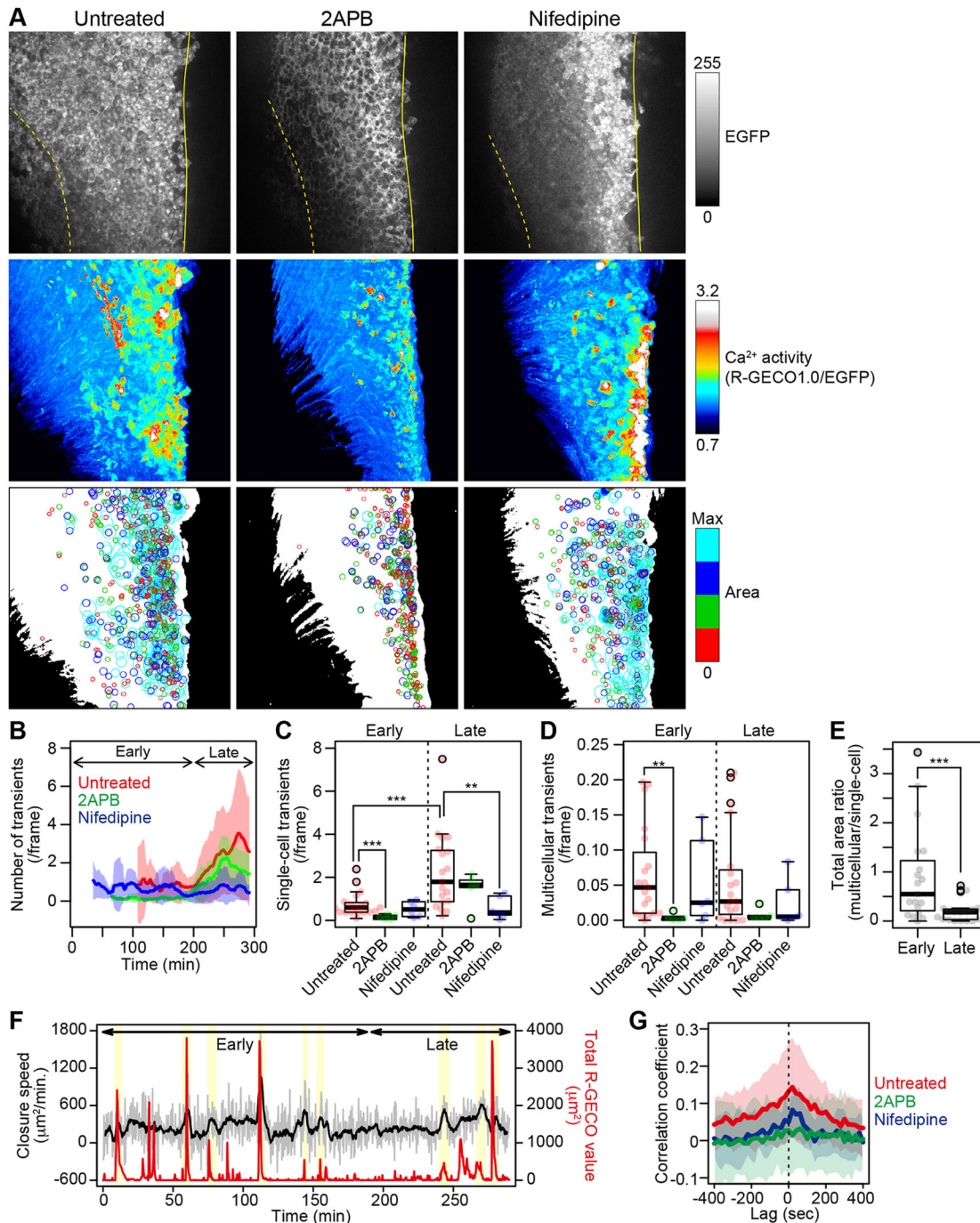


**Fig. 3. Quantitative analyses of intracellular  $\text{Ca}^{2+}$  activities in the neural plate.** (A) Representative results of quantitative analyses of a  $\text{Ca}^{2+}$  fluctuation in an untreated (left), 2APB-treated (middle) and nifedipine-treated (right) embryo. R-GECO1.0 and EGFP were introduced into the left side of the NPs. (Top) EGFP fluorescence images at the start of time-lapse recording; (middle) time projections of  $\text{Ca}^{2+}$  activity (R-GECO1.0/EGFP); and (bottom) time projections of reconstructed circles corresponding to the area of the  $\text{Ca}^{2+}$  transient, extracted by image processing. Solid yellow lines indicate the midline; dotted lines indicate the border between neural and non-neural tissues. The reconstructed circles were color-coded based on the quartiles of the area distributions in an untreated embryo. (B) The mean number of  $\text{Ca}^{2+}$  transients during NTC. The time interval of observations was 20 s. The data are shown as smoothed curves, obtained by averaging the originally counted numbers at a given time point with those of neighboring time points (50 time points total). The shaded area indicates the s.d. (C) The number of single-cell  $\text{Ca}^{2+}$  transients in the early and late phases of NTC.  $**P < 0.01$  and  $***P < 0.001$ , two-sided Mann–Whitney  $U$ -test. (D) The number of multicellular  $\text{Ca}^{2+}$  transients in the early and late phases of NTC.  $**P < 0.01$ , two-sided Mann–Whitney  $U$ -test. (E) The ratio of the total area of the multicellular or single-cell  $\text{Ca}^{2+}$  transients in the early and late phases of NTC in untreated embryos.  $***P < 0.001$ , two-sided Wilcoxon signed rank test. (F) Representative data for the closing speed (black) and the total R-GECO1.0 intensity values at the tissue level (red) during NTC. The closing speed is shown as a smoothed curve, obtained by averaging the rate determined from image analyses (gray) at a given time point with those of neighboring time points (ten time points total). Overlaps between temporary increases in closing speed and intense  $\text{Ca}^{2+}$  transients are highlighted (yellow). (G) Mean cross-correlation coefficients between the closing speed and the total R-GECO1.0 value. The shaded area indicates s.d.  $n = 19$  (untreated), 5 (2APB-treated) and 6 (nifedipine-treated) embryos. Results in B–E and G are for the same data set. In C–E, the box and whiskers of these plots indicate maximum, third quarter, median, first quarter and minimum values of each group, respectively, from upper side to the bottom of the graphs. Data beyond the end of the whiskers, the upper limit of whiskers is 1.5 times the box length, are shown as outliers.

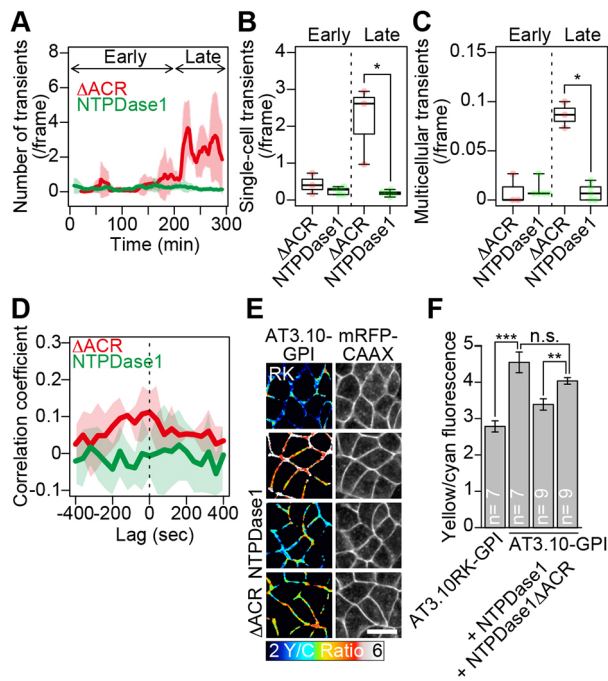


**Fig. 4. Extracellular ATP in  $\text{Ca}^{2+}$  fluctuations and NTC.** (A) Mean number of  $\text{Ca}^{2+}$  transients in embryos expressing an E-NTPDase1 mutant ( $\Delta\text{ACR}$ ; red) or E-NTPDase1 (NTPDase1; green), shown as smoothed curves obtained by averaging the originally counted values at a given time point with those of neighboring time points (25 time points total). Time interval of observations is 40 s. Shaded area indicates the s.d. (B) Number of single-cell  $\text{Ca}^{2+}$  transients in the early and late phases of NTC. \* $P < 0.05$ , two-sided Mann–Whitney  $U$ -test. (C) Number of multicellular  $\text{Ca}^{2+}$  transients in the early and late phases of NTC. \* $P < 0.05$ , two-sided Mann–Whitney  $U$ -test. (D) The mean cross-correlation between the closing speed and the total R-GECO1.0 value in embryos expressing a mutant E-NTPDase1 ( $\Delta\text{ACR}$ ; red) or E-NTPDase1 (NTPDase1; green). The shaded area indicates s.d.  $n = 3$  ( $\Delta\text{ACR}$ ), 5 (NTPDase1) embryos. Results in A–D are for the same data set. (E) Images showing the yellow-to-cyan (yellow/cyan; Y/C) fluorescence ratio value of AT3.10RK-GPI (top, control), AT3.10-GPI (second to bottom) on the surface of NP cells, by FRET analysis (left). The mean ratio was measured from the masked region generated by membrane-targeted mRFP (right). Scale bar: 30  $\mu\text{m}$ . (F) The mean yellow-to-cyan fluorescence ratio value of AT3.10-GPI on cell surfaces in the NP by FRET analysis. The number of embryos examined is indicated in each bar. Error bars show s.e.m. \*\* $P < 0.01$  and \*\*\* $P < 0.001$ , two-sided Welch’s  $t$ -test. n.s., not significant. In B and C, the box and whiskers of these plots indicate maximum, third quarter, median, first quarter and minimum values of each groups, respectively, from upper side to the bottom of the graphs.

eATP in  $\text{Ca}^{2+}$  fluctuations using the fluorescence resonance energy transfer (FRET)-based ATP indicator ATeam3.10 (see Supplementary Materials and Methods) (Imamura et al., 2009). We found that extracellularly expressed ATeam3.10 increased the ratio of yellow-to-cyan fluorescence on the cell membrane compared with a mutant form of ATeam3.10 that is unable to bind to ATP (RK mutant) (Fig. 4E,F). Co-expressing E-NTPDase1 suppressed this increase in the ratio of yellow-to-cyan fluorescence but co-expressing the  $\Delta\text{ACR}$  variant did not (Fig. 4E,F). Taken together, these data suggest that eATP exists in the NP and regulates the  $\text{Ca}^{2+}$  fluctuations.

#### **$\text{Ca}^{2+}$ transients induce cortical F-actin remodeling and AC**

$\text{Ca}^{2+}$  fluctuations in the embryo regulate various cellular behaviors, such as cell flattening (Markova and Lenne, 2012), cell intercalation and polarization (Shindo et al., 2010; Wallingford et al., 2001), and cell contraction (Hunter et al., 2014). In addition, during wound

healing in the developing epidermis, multicellular wave-like  $\text{Ca}^{2+}$  transients accelerate the closure process through cell shape changes (Antunes et al., 2013; Herrgen et al., 2014), suggesting that  $\text{Ca}^{2+}$ -mediated cellular mechanisms underlie tissue development and homeostasis through epithelial remodeling. We investigated the relationship between  $\text{Ca}^{2+}$  fluctuations and NTC at the cellular level by simultaneously imaging R-GECO1.0 and the F-actin marker Lifeact-EGFP, which marks the cell periphery (Riedl et al., 2008). We found that immediately after a  $\text{Ca}^{2+}$  transient, mesh-like F-actin structures developed in the center of the cell and were maintained for several minutes, even after the  $\text{Ca}^{2+}$  had dropped back to basal levels within a few tens of seconds (Fig. 5A, +60 s to +160 s, and B; Movie 4). Furthermore, the area of the apical side of the NP cells decreased rapidly and then stabilized within a minute after a  $\text{Ca}^{2+}$  transient (Fig. 5A,B; Movie 4). Cross-correlation analyses among the R-GECO1.0 values, medial F-actin and cell area dynamics revealed that the maximum correlation with the F-actin signals was obtained at time lag 0, whereas with the cell area dynamics, it occurred when the R-GECO1.0 value was shifted later in time (Fig. 5C), which corresponded with tissue-level analysis (Fig. 3G). These data suggest that the rapid activation and prolonged F-actin remodeling induced by  $\text{Ca}^{2+}$  may be the mechanism of AC and NTC by which relaxation to the original state (i.e. before  $\text{Ca}^{2+}$  transients occurred) is suppressed. We could not determine whether the  $\text{Ca}^{2+}$ -induced F-actin remodeling was due to overall polymerization or to the relocalization of F-actin to the apical side; both processes are implicated in the rapid cell contractions during *Drosophila* mesodermal invagination (Mason et al., 2013). In addition, it is also possible that non-muscle myosin II is activated by  $\text{Ca}^{2+}$  transients through known pathways such as calmodulin-dependent kinase (CaMKII)-mediated RhoA (Murakoshi et al., 2011) and myosin light chain kinase (MLCK) activation (Vicente-Manzanares et al., 2009).

We addressed the causal relationship between the  $\text{Ca}^{2+}$  transient and AC by using 1-(2-nitrophenyl)ethyl (NPE)-caged inositol triphosphate ( $\text{IP}_3$ ) and 1-(4,5-dimethoxy-2-nitrophenyl)ethyl (DMNPE)-caged ATP to experimentally induce  $\text{Ca}^{2+}$  transients. Brief ultraviolet (UV) illumination applied to an embryo that had been injected with NPE-caged  $\text{IP}_3$  induced a localized  $\text{Ca}^{2+}$  transient (Movie 5), followed by a decrease in the apical-side area of the UV-illuminated NP cells compared with that of unilluminated cells (Fig. 5D). Furthermore, by uncaging DMNPE-caged ATP applied to the ringer solution, we induced an intense multicellular  $\text{Ca}^{2+}$  propagation wave followed by the shrinkage of NP cells at the tissue level (Fig. 5E; Movies 6 and 7). Since F-actin in the medial region is linked to the junctional cadherin complexes during AC (Martin and Goldstein, 2014; Mason et al., 2013; Sawyer et al., 2010), we focused on N-cadherin (*cdh2*), which is required for F-actin assembly in the NP (Morita et al., 2010; Nandadasa et al., 2009). We found that blocking the function of N-cadherin in DMNPE-caged ATP-stimulated NP cells inhibited the decrease in apical area (Fig. 5E; Movies 8 and 9). These data suggest that the  $\text{Ca}^{2+}$  transients induce AC in NP cells, and that N-cadherin plays a role in the  $\text{Ca}^{2+}$ -induced AC.

#### **Mathematical analysis of NTC based on pulsed apical contraction**

Our experimental results raise the possibility that the  $\text{Ca}^{2+}$  fluctuations function to decrease the total apical area of the NP. It is possible that  $\text{Ca}^{2+}$  fluctuations modulate cellular properties or mechanical processes. Indeed, we have demonstrated that  $\text{Ca}^{2+}$  fluctuations appear to regulate the localization of F-actin, which is

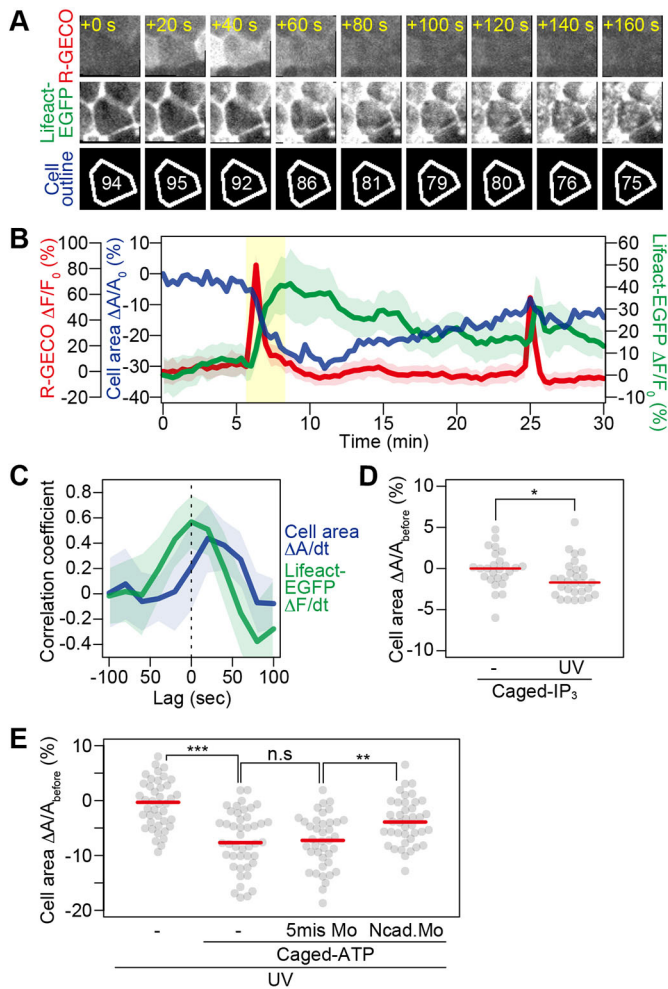


**Fig. 5. Relationship between  $\text{Ca}^{2+}$  fluctuation and AC.** (A) Dynamics of intracellular  $\text{Ca}^{2+}$  and F-actin at the single-cell level. An embryo expressing R-GECO1.0 (top) and Lifeact-EGFP (middle) was imaged during NTC. The numbers in the top panels (+0–160) indicate time (seconds) corresponding to the 340–500 s range in B (yellow in B). Numbers shown in the cell outlines (bottom) indicate the apical cell area (%) relative to that at time 0 in B. (B) Temporal profiles of the mean fluorescent intensities ( $\Delta F/F_0$ ) of R-GECO1.0 (red) and medial Lifeact-EGFP (green), and the relative apical cell area (blue;  $\Delta A/A_0$ ) in a single cell. The shaded areas indicate the s.d. The time period represented in A is highlighted in yellow. (C) Mean cross-correlation coefficients between the temporal dynamics of the apical cell area (blue), medial Lifeact-EGFP (green) and R-GECO1.0 ( $n=8$  transients, 4 cells, 1 embryo). The shaded areas indicate s.d. (D) Relative apical cell area 50 s after photolysis of NPE-caged  $\text{IP}_3$  in the NP. Red line indicates the median value.  $*P<0.05$ , two-sided Mann–Whitney  $U$ -test;  $n=26$  cells, 2 embryos (–UV); 29 cells, 2 embryos (+UV). (E) Relative apical cell area 50 s after photolysis of DMNPE-caged ATP in the NP. Red line indicates the median value.  $**P<0.01$  and  $***P<0.001$ , two-sided Mann–Whitney  $U$ -test;  $n=42$  cells, 4 embryos (–DMNPE-caged ATP); 44 cells, 4 embryos (+DMNPE-caged ATP); 39 cells, 4 embryos (5mis-N-cadherin Mo; +DMNPE-caged ATP); 40 cells, 4 embryos (N-cadherin Mo; +DMNPE-caged ATP). 5mis, missense; Mo, morpholino; n.s., not significant.

involved in regulating both cell properties and mechanical processes. There are two types of transient  $\text{Ca}^{2+}$  fluctuations: those that occur at the single-cell level, and those that occur at the multicellular level. In order to evaluate differences in the effect and function of each type of  $\text{Ca}^{2+}$  fluctuation at the cellular level on tissue deformation, we constructed a multi-cell-based mechanical model, in which the  $\text{Ca}^{2+}$  fluctuations modulate a cellular

mechanical parameter of a simplified epithelial tissue (Fig. 6A; Supplementary Materials and Methods). Our model is based on the vertex model, which is a well-known mathematical framework used to describe multicellular tissue dynamics (Farhadifar et al., 2007; Nagai and Honda, 2001; Okuda et al., 2013; Rauzi et al., 2008). To examine how the transient and patterned modulation of mechanical processes or properties in the cell results in the persistent shrinkage of an epithelial sheet, we introduced two components to our model. The first is the mechanical effect of the  $\text{Ca}^{2+}$  transient as a modification of the line tension of the cellular edges over a short time period (Fig. 6B), which is expected to decrease the cell surface area (see Supplementary Materials and Methods for definition). The second is the constrictive nature of the apical cell surface with a ratchet effect (Fig. 6C,D): the cells' natural surface area and the cells' natural perimeter are permitted to decrease but not to increase (see Supplementary Materials and Methods for definition). In our model, by regulating the spatial and temporal pattern of the modification of the line tensions, the effect of the  $\text{Ca}^{2+}$  transient at the single-cell and the multicellular levels can be simulated. Furthermore, the regulations of the cells' natural surface area and the cells' natural perimeter enabled us to introduce a ratchet-like mechanism (Martin and Goldstein, 2014; Mason et al., 2013; Sawyer et al., 2010) that has not been previously introduced (Spahn and Reuter, 2013).

Using this model, we first examined the combined effect of the  $\text{Ca}^{2+}$  transient (pulse) and the constrictive nature of apical cell surface (Acn) on the modeled epithelial tissue. Without either of these components and with the pulse component alone, the tissue size rarely changed at the end of the simulation time (Fig. 7A,B). Interestingly, adding the Acn component caused the modeled tissue to gradually decrease in size, and the combination of pulse and Acn components accelerated such decreasing behavior (Fig. 7A,B; Movie 10). At the single-cell level, transiently increased potential energies of apical surface area and perimeter, which were induced by modification of line tension during a single pulse, led to contraction of apical surface area and perimeter, respectively (Fig. 7C; Fig. S4). When the Acn component existed, those contractions further resulted in the irreversible decrease of the natural surface area and the natural perimeter (Fig. 7C; Fig. S4). Interestingly, after the contractions of apical cell surface area and perimeter that were induced by the pulse, a considerable relaxation event also occurred (Fig. 7C; Fig. S4), which were indeed observed during an AC event after a single  $\text{Ca}^{2+}$  transient *in vivo* (Fig. 5B). These results suggest that our model reproduces the *in vivo* situation, in which  $\text{Ca}^{2+}$  transients accelerate AC and, hence, decreases the tissue size when the stabilization mechanisms are present.

Next, in order to examine the role of  $\text{Ca}^{2+}$  transients in decreasing tissue size qualitatively, we gradually changed the pulse number and found that the effect became more pronounced as the total number of pulses was increased independently of the proportion of activated edges per cell (Fig. 7D). Under simulation with sparse pulses, the relationship between the number of pulses and the constriction rate showed a nearly linear dependence (Fig. S6). Next, we concentrated on the spatial and temporal frequencies of the pulse to examine the collective effect. In comparing dense versus sparse pulses, we found that dense pulses induced tissue deformation more rapidly within the active period (Fig. 7E,G). However, over the entire course of the simulation, dense pulses were less effective than sparse pulses when the same total number of pulses was used (Fig. 7E,F; Movie 11). The negative effect of pulse collectivity on the decrease in tissue size was attenuated as the proportion of activated edges per cell was decreased (Fig. 7F). However, because almost all of the segments

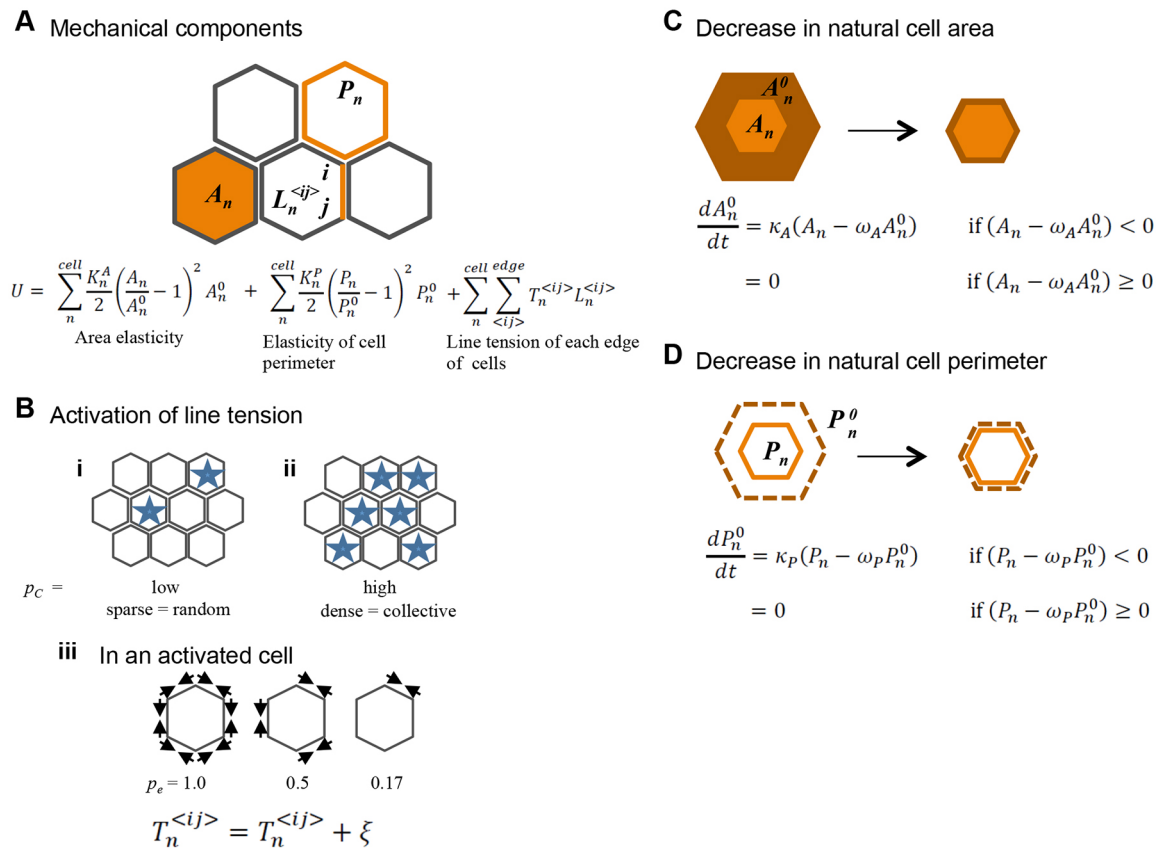


**Fig. 6. Schematic representation of the vertex model.** (A) The mechanical potentials are shown with five cells. (B) Effect of the  $\text{Ca}^{2+}$  transient is described. The  $\text{Ca}^{2+}$  transients at the single-cell (i) and multicellular (ii) levels are shown. Cells marked by blue stars are activated. Activated cellular edges in an activated cell are marked by arrows (iii). (C,D) The constrictive nature of the apical cell surface with a ratchet-like stabilization is modeled by two differential equations. The regulation of the natural cell area and of the natural cell perimeter are described in C and D, respectively. The bright orange regions in C are the actual cell surface area, and the dark orange regions correspond to the natural cell surface area. The bright orange lines in D are the actual cell perimeter, and the dark orange broken lines correspond to the natural perimeter. See main text and Supplementary Materials and Methods for the detail.

contract in the *in vivo* situation (Fig. 5A), these data suggest that random  $\text{Ca}^{2+}$  fluctuations at the single-cell level decrease the tissue size more effectively than multicellular collective  $\text{Ca}^{2+}$  fluctuations.

In order to examine the robustness of the above results, we analyzed the modified models with varied assumptions (Fig. S5). When the coefficients of elasticity of a cell's apical surface and apical perimeter were assumed to decrease during the pulse, the effectiveness of sparse pulses on decreasing tissue size was observed in the presence of the Acn component (Fig. S5A), similar to when the pulse was linked to activation of line tension (Fig. 7E). On the other hand, when the tension fluctuation was induced during the pulse, the decrease in tissue size was not accelerated (Fig. S5B). As another attempt, we analyzed the two modified models in which the natural/preferred area was allowed to increase. The results showed that the effectiveness of sparse pulses on decreasing tissue size was also observed in the presence of the Acn component, although the differences in the constriction rate became smaller (Fig. S5C,D). These data suggest that under the conditions that recapitulate the combinational effects *in vivo*, the prediction regarding the effectiveness of sparse pulses on decreasing tissue size was robust.

In order to validate the prediction from the model simulations *in vivo*, we fitted a linear mixed model with single-cell and multicellular  $\text{Ca}^{2+}$  transients as explanatory variables and the amount of NTC as a response variable to data of untreated embryos, and obtained estimated contributions of single-cell  $\text{Ca}^{2+}$  transients

and multicellular  $\text{Ca}^{2+}$  transients to the amount of NTC (Fig. S7 and Supplementary Materials and Methods). As is shown in Table 1, the coefficient of single-cell  $\text{Ca}^{2+}$  transients ( $0.072 \pm 0.011$ ; estimated mean  $\pm$  s.e.m.) was significantly larger than that of multicellular  $\text{Ca}^{2+}$  transients ( $0.028 \pm 0.011$ ) ( $P$ -value =  $7.231 \times 10^{-3}$ , Student's  $t$ -test). These results support the prediction from the model simulations that the  $\text{Ca}^{2+}$  fluctuations at the single-cell level more effectively accelerate AC and NTC than multicellular  $\text{Ca}^{2+}$  fluctuations do *in vivo*.

## DISCUSSION

In this study, we show that two types of active  $\text{Ca}^{2+}$  signaling patterns modulate AC via cortical F-actin remodeling, and thereby contribute differently to efficient NTC. Our present study and a recent paper (Christodoulou and Skourides, 2015) propose a new role of active  $\text{Ca}^{2+}$  fluctuation in accelerating AC. The trigger for  $\text{Ca}^{2+}$  transients and the mechanism that allow it to propagate through a tissue remain to be investigated. We did not detect any bias in the direction of wave propagation relative to the body axes, whereas the wave propagation in the wound healing response has previously been shown to originate from wounded cells (Antunes et al., 2013; Herrgen et al., 2014). Multicellular  $\text{Ca}^{2+}$  transients in the NP produced a higher intensity of R-GECO1.0 fluorescence per cell than did single-cell level transients (Fig. 2); therefore, the wave-like propagation of  $\text{Ca}^{2+}$  transients at the tissue level might be induced above a particular threshold  $\text{Ca}^{2+}$  signal strength. Our study

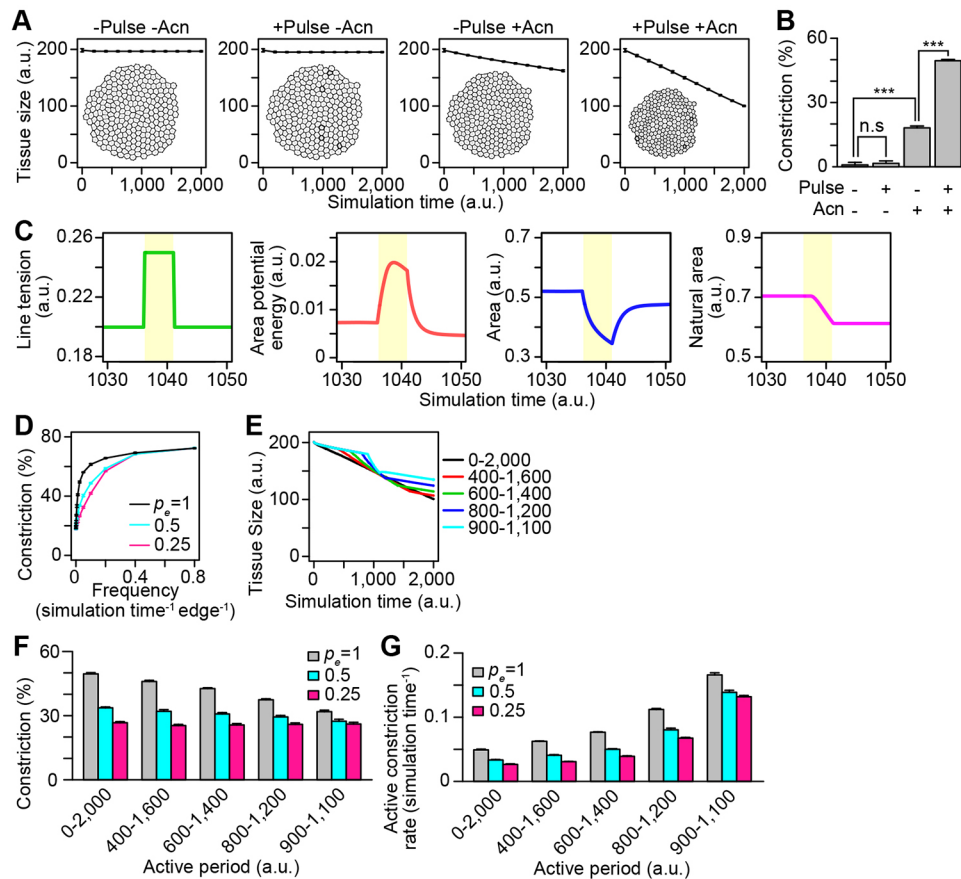


**Fig. 7. Mathematical analysis of pulsed AC.** (A) Mean tissue sizes of the modeled epithelial sheets during the time course of the simulations, and representative images at the end of each simulation. (B) Mean tissue constriction at the end of the simulations. In A and B, the pulsed contractions were introduced at a frequency of  $0.025 \text{ simulation time}^{-1} \text{ edge}^{-1}$ , and all of the cell edges in the activated cells were contracted.  $***P < 0.001$ , two-sided Student's *t*-test. n.s., not significant. (C) Mean line tension, potential energy from the elasticity of apical surface area, area and natural area of single cell (#58) during the time course of the simulations with the pulse and Acn components. The period with pulse is highlighted in yellow. See Supplementary Materials and Methods for definitions. (D) Relationship between the pulse frequency and mean constriction at the end of the simulations. The proportion of cell edges undergoing contraction per cell was set to a probability ( $p_e$ ) of 1, 0.5 or 0.25. (E) Mean tissue sizes during the time course of the simulations, when the active period in which the pulses were introduced was set from 200 to 2000 simulation times. (F,G) The mean constriction at the end of the simulations and the constriction rate during the active period, when the length of the active period and the proportion of the cell edges undergoing contraction per cell were changed. All error bars depict s.d.;  $n=5$  different initial conditions. Details of the models and of the simulation processes are described in the supplementary Materials and Methods, Tables S1 and S2.

also suggests that eATP regulates both the single-cell and the multicellular  $\text{Ca}^{2+}$  transients (Fig. 4). eATP activates downstream signaling in the cell that secreted the ATP (autocrine signaling) and in neighboring cells (paracrine signaling) (Corriden and Insel, 2010; Schwiebert and Zsembery, 2003). Several pathways, including ATP-permeable release channels and ATP-filled vesicles have been proposed to secrete cytosolic ATP, which is triggered by mechanical stimulation or extracellular biochemical cues (Corriden and Insel, 2010; Schwiebert and Zsembery, 2003). Hence, ATP release induced by spontaneous mechanical stretch or

compression might trigger  $\text{Ca}^{2+}$  transients and possibly the wave propagation in the developing NP, in which dynamic autonomous and non-autonomous tissue movements take place (Morita et al., 2012; Wallingford and Harland, 2001). In order to dissect more precisely the regulatory mechanisms upstream of  $\text{Ca}^{2+}$  transients, functional studies using genome editing, for example, would be useful since pharmacological approaches can be misleading due to off-target effects (Bootman et al., 2002; Xu et al., 2005).

Although multicellular  $\text{Ca}^{2+}$  transients have been shown to accelerate closure process during wound healing (Antunes et al.,

**Table 1. Statistics for fixed effects of the mixed linear model**

Explanatory variables	Median value	First quartile ( $Q_1$ )	Third quartile ( $Q_3$ )	Estimated mean	s.e.m.	Degrees of freedom	<i>t</i> -value	<i>P</i> -value
Intercept				4554	380.7	358	11.96	$5.655 \times 10^{-28}$
Single-cell $\text{Ca}^{2+}$ transients	4552*	2088*	12444*	0.07210	0.01108	358	6.505	$2.626 \times 10^{-10}$
Multicellular $\text{Ca}^{2+}$ transients	2811*	1125*	8145*	0.02820	0.01075	358	2.624	$9.060 \times 10^{-3}$
Time window number	10.5	5.75	15.25	40.68	24.01	358	1.694	$9.108 \times 10^{-2}$

\*Values of zero were excluded for calculation.



2013; Herrgen et al., 2014), the contribution of random single-cell  $\text{Ca}^{2+}$  fluctuations to epithelial remodeling has been elusive, probably because the effect of these transients is too small at the tissue level to be examined experimentally. Moreover, since the temporal patterns of single-cell  $\text{Ca}^{2+}$  fluctuations varied among embryos (Fig. 3B–E), it might be regulated by mechanisms that are inherently noisy or heterogenous, further complicating efforts to draw general conclusions about its functional significance. In this study, we used a cell-vertex mathematical model in surface view to investigate how distinct  $\text{Ca}^{2+}$  fluctuation patterns affect AC and persistent epithelial remodeling (Figs 6 and 7). Computational simulations using this model showed that pulsed contractions accelerate the decrease in tissue size, even when pulses occurred with a sparse frequency, suggesting that  $\text{Ca}^{2+}$ -induced AC always contributes positively to NTC. Our mathematical and statistical analyses also suggest that spatially and temporally random  $\text{Ca}^{2+}$  transients at the single-cell level function to reduce the overall tissue size more effectively than multicellular collective  $\text{Ca}^{2+}$  fluctuations, making them cost-effective for normal NTC. On the other hand, the multicellular wave-propagated  $\text{Ca}^{2+}$  transients might be useful when a tissue must be closed quickly, as in wound healing. Since the number of single-cell  $\text{Ca}^{2+}$  transients increases in the late phase of NTC, a genetic program that represses collectivity and promotes the randomization of  $\text{Ca}^{2+}$  fluctuations might exist to ensure that embryos are able to undertake their primitive CNS formation under physiological conditions. In summary, the  $\text{Ca}^{2+}$ -dependent mechanisms highlighted in this study might be acting in parallel with known pathways that control AC, such as the Shroom3 or Wnt/PCP pathway, as a compensatory system to avoid incomplete NTC, which is the second most frequent congenital malformation in humans (Copp et al., 2003).

## MATERIALS AND METHODS

### Ethics statement

All protocols for animal care and experiments were approved by the Institutional Animal Care and Use Committee of the National Institutes of Natural Sciences, Japan, and were performed in accordance with institutional guidelines for the care and use of laboratory animals.

### Injections, morpholinos and RNA expression constructs

Experiments with *Xenopus laevis* embryos were performed as previously described (Suzuki et al., 2010). After injection, the embryos were cultured in 3% Ficoll with 0.1× Steinberg's solution until stage 9, then washed and cultured in 0.3× Marc's Modified Ringer's medium (MMR) until the appropriate stage for analysis (Nieuwkoop and Faber, 1967).

Antisense morpholino (Gene Tools) was injected into embryos at the four-cell stage (17 ng per embryo). The morpholino sequences were as follows: N-cadherin morpholino 5'-GAAGGGCTCTTTCCGGCACATGGTG-3' (Nandadasa et al., 2009); 5mis-N-cadherin morpholino, 5'-GAACGGGTCTTTGCGCCACATCGTG-3'.

Capped sense RNAs were synthesized with the mMACHINE mMACHINE kit (Ambion), purified on a NICK column (GE Healthcare) and injected into embryos at the four-cell stage. All open reading frames were cloned into the pCS2p+ vector. Embryos received injections of RNA constructs in the following amounts: R-GECO1.0 (Zhao et al., 2011) and G-GECO1.2 (Zhao et al., 2011), 1 ng per embryo; YC-Nano50 (Horikawa et al., 2010), YC-Nano30 (Horikawa et al., 2010) and YC-Nano15 (Horikawa et al., 2010), 500 pg per embryo. Cell surface-targeted ATeam3.10 (AT3.10-GPI) and its RK mutant were generated by fusing ATeam3.10 (Imamura et al., 2009) or its RK mutant (Imamura et al., 2009) with the signal peptide sequence and the GPI-anchor domain of *Xenopus* glypican4 (Ohkawara et al., 2003), and 1 ng was injected per embryo. EGFP was injected at 100 pg per embryo. Membrane-targeted EGFP and mRFP were generated by fusing the farnesylation signal of c-Ha-Ras to the

C terminus of EGFP and mRFP, respectively, and 100–200 pg was injected per embryo. Lifeact-EGFP (Riedl et al., 2008) was injected at 180 pg per embryo. *Xenopus* E-NTPDase1 and its mutant version, in which the enzymatic active site had been deleted ( $\Delta\text{ACR}$ ), were injected at 100–200 pg per embryo.

### Chemical treatments

For inhibitor treatments, 100× stocks of 2APB (D9754; Sigma) and nifedipine (145-05781; Wako) in DMSO were added to the medium at stage 13, to concentrations of 25  $\mu\text{M}$  and 200  $\mu\text{M}$ , respectively. For uncaging experiments, NPE-caged  $\text{IP}_3$  (I23580; Molecular Probes) was injected into embryos at the four-cell stage (5 pmol per embryo). DMNPE-caged ATP (A1049; Molecular Probes) was added to the medium to a concentration of 100  $\mu\text{M}$ .

### In situ hybridization and F-actin staining

*In situ* hybridization was performed as previously described (Suzuki et al., 2010). The following plasmids were used for probe synthesis: *Sox2* (XL039o24; XDB3); *N-cadherin* (XL289n05ex; XDB3); and *Epidermal keratin* (XL056e18; XDB3). For F-actin visualization, embryos were fixed in MOPS, EGTA, magnesium sulfate, formaldehyde buffer (MEMFA) and stained with Alexa 546-phalloidin (A22283; Molecular Probes).

### Confocal imaging

Devitelinized embryos were mounted on an agarose-coated glass-based dish (3910-035; AGC, Japan) filled with 0.3× MMR. Confocal fluorescence images were acquired as a z-series of 512×512 pixels using a spinning-disc confocal unit (CSU-X1; Yokogawa, Japan) with an EMCCD camera (iXon3; Andor) and 455-, 488- and 561-nm lasers (Andor) on an inverted microscope (IX81; Olympus) with a 10× (UPlanSAPO 10×/0.4; Olympus) or 20× (UPlanAPO 20×/0.7; Olympus) objective lens at a room temperature adjusted to 18–20°C. Unless otherwise noted, we observed the R-GECO1.0 fluorescence at 20 or 40 s intervals for up to 6 h.

For UV illumination in uncaging experiments, mercury lamp-based epifluorescent optics with a band-pass filter (AT350/50×; Chroma) were inserted into the path of the excitation light, and the duration of illumination was controlled by iQ2 software (Andor). For the photolysis of NPE-caged  $\text{IP}_3$ , the samples were illuminated for 3 s by a UV light reduced with a 6% neutral-density filter (32-ND6; Olympus). For the photolysis of DMNPE-caged ATP, the samples were illuminated for 20 s by unreduced UV light.

Image processing and analyses were performed using ImageJ (NIH) and R ([www.r-project.org](http://www.r-project.org)) software. All quantifications used the maximum intensity projection of the z-series. Details are provided in Supplementary Materials and Methods.

### Mathematical model

The mathematical model constructed in this study is based on the vertex model (Farhadifar et al., 2007; Nagai and Honda, 2001; Okuda et al., 2013; Rauzi et al., 2008). The simulations were programmed in C. Details are provided in Supplementary Materials and Methods.

### Illustrations and statistical analyses

Figures were assembled with Photoshop (Adobe), Illustrator (Adobe) and PowerPoint (Microsoft). Data plots and statistical analyses were performed in Excel (Microsoft) and R software. Data sets were subjected to Shapiro–Wilk's test to determine distributions. No statistical method was used to predetermine sample size. The experiments were not randomized. The investigators were not blinded to allocation during experiments and outcome assessment.

### Acknowledgements

We thank the Data Integration and Analysis Facility, and the Spectrography and Bioimaging Facility in the National Institute for Basic Biology Core Research Facilities for technical support; members of the N.U. laboratory, S. Nonaka laboratory and N. Shiina laboratory for valuable discussions and comments.

### Competing interests

The authors declare no competing or financial interests.

## Author contributions

M. Suzuki, M. Sato, H.K., Y.H., T.F. and N.U. designed research; M. Suzuki, H.K., Y.H. and N.Y. performed research; M. Suzuki, M. Sato., H.K., K.H., H.I., T.N. and R.E.C. contributed new reagents and analytical tools; M. Suzuki., M. Sato, H.K., Y.H. and N.Y. analyzed the data; and M. Suzuki, M. Sato, H.K., R.E.C. and N.U. wrote the paper.

## Funding

This work was supported by KAKENHI [23770261 and 15KT0154 to M.S., 22127007 and 15H05865 to N.U.] from the Japan Society for the Promotion of Science (JSPS).

## Supplementary information

Supplementary information available online at <http://dev.biologists.org/lookup/doi/10.1242/dev.141952.supplemental>

## References

- Antunes, M., Pereira, T., Cordeiro, J. V., Almeida, L. and Jacinto, A.** (2013). Coordinated waves of actomyosin flow and apical cell constriction immediately after wounding. *J. Cell Biol.* **202**, 365-379.
- Bootman, M. D., Collins, T. J., Mackenzie, L., Roderick, H. L., Berridge, M. J. and Peppiatt, C. M.** (2002). 2-aminoethoxydiphenyl borate (2-APB) is a reliable blocker of store-operated Ca<sup>2+</sup> entry but an inconsistent inhibitor of InsP<sub>3</sub>-induced Ca<sup>2+</sup> release. *FASEB J.* **16**, 1145-1150.
- Christodoulou, N. and Skourides, P. A.** (2015). Cell-autonomous Ca(2+) flashes elicit pulsed contractions of an apical actin network to drive apical constriction during neural tube closure. *Cell Rep.* **13**, 2189-2202.
- Clapham, D. E.** (2007). Calcium signaling. *Cell* **131**, 1047-1058.
- Copp, A. J., Greene, N. D. E. and Murdoch, J. N.** (2003). The genetic basis of mammalian neurulation. *Nat. Rev. Genet.* **4**, 784-793.
- Corriden, R. and Insel, P. A.** (2010). Basal release of ATP: an autocrine-paracrine mechanism for cell regulation. *Sci. Signal.* **3**, re1.
- Farhadifar, R., Röper, J.-C., Aigouy, B., Eaton, S. and Jülicher, F.** (2007). The influence of cell mechanics, cell-cell interactions, and proliferation on epithelial packing. *Curr. Biol.* **17**, 2095-2104.
- Ferreira, M. C. and Hilfer, S. R.** (1993). Calcium regulation of neural fold formation: visualization of the actin cytoskeleton in living chick embryos. *Dev. Biol.* **159**, 427-440.
- Guillot, C. and Lecuit, T.** (2013). Mechanics of epithelial tissue homeostasis and morphogenesis. *Science* **340**, 1185-1189.
- Herrgen, L., Voss, O. P. and Akerman, C. J.** (2014). Calcium-dependent neuroepithelial contractions expel damaged cells from the developing brain. *Dev. Cell* **31**, 599-613.
- Horikawa, K., Yamada, Y., Matsuda, T., Kobayashi, K., Hashimoto, M., Matsuura, T., Miyawaki, A., Michikawa, T., Mikoshiba, K. and Nagai, T.** (2010). Spontaneous network activity visualized by ultrasensitive Ca(2+) indicators, yellow Cameleon-Nano. *Nat. Methods* **7**, 729-732.
- Hunter, G. L., Crawford, J. M., Genkins, J. Z. and Kiehart, D. P.** (2014). Ion channels contribute to the regulation of cell sheet forces during Drosophila dorsal closure. *Development* **141**, 325-334.
- Imamura, H., Nhat, K. P., Togawa, H., Saito, K., Iino, R., Kato-Yamada, Y., Nagai, T. and Noji, H.** (2009). Visualization of ATP levels inside single living cells with fluorescence resonance energy transfer-based genetically encoded indicators. *Proc. Natl. Acad. Sci. USA* **106**, 15651-15656.
- Kim, Y., Hazar, M., Vijayraghavan, D. S., Song, J., Jackson, T. R., Joshi, S. D., Messner, W. C., Davidson, L. A. and LeDuc, P. R.** (2014). Mechanochemical actuators of embryonic epithelial contractility. *Proc. Natl. Acad. Sci. USA* **111**, 14366-14371.
- Leclerc, C., Webb, S. E., Daguzan, C., Moreau, M. and Miller, A. L.** (2000). Imaging patterns of calcium transients during neural induction in *Xenopus laevis* embryos. *J. Cell Sci.* **113**, 3519-3529.
- Lee, H. and Nagele, R. G.** (1986). Toxic and teratologic effects of verapamil on early chick embryos: evidence for the involvement of calcium in neural tube closure. *Teratology* **33**, 203-211.
- Markov, O. and Lenne, P.-F.** (2012). Calcium signaling in developing embryos: focus on the regulation of cell shape changes and collective movements. *Semin. Cell Dev. Biol.* **23**, 298-307.
- Martin, A. C. and Goldstein, B.** (2014). Apical constriction: themes and variations on a cellular mechanism driving morphogenesis. *Development* **141**, 1987-1998.
- Mason, F. M., Tworoger, M. and Martin, A. C.** (2013). Apical domain polarization localizes actin-myosin activity to drive ratchet-like apical constriction. *Nat. Cell Biol.* **15**, 926-936.
- Massé, K., Bhamra, S., Eason, R., Dale, N. and Jones, E. A.** (2007). Purine-mediated signalling triggers eye development. *Nature* **449**, 1058-1062.
- Moran, D. and Rice, R. W.** (1976). Action of papaverine and ionophore A23187 on neurulation. *Nature* **261**, 497-499.
- Morita, H., Nandadasa, S., Yamamoto, T. S., Terasaka-Iioka, C., Wylie, C. and Ueno, N.** (2010). Nectin-2 and N-cadherin interact through extracellular domains and induce apical accumulation of F-actin in apical constriction of *Xenopus* neural tube morphogenesis. *Development* **137**, 1315-1325.
- Morita, H., Kajiura-Kobayashi, H., Takagi, C., Yamamoto, T. S., Nonaka, S. and Ueno, N.** (2012). Cell movements of the deep layer of non-neural ectoderm underlie complete neural tube closure in *Xenopus*. *Development* **139**, 1417-1426.
- Murakoshi, H., Wang, H. and Yasuda, R.** (2011). Local, persistent activation of Rho GTPases during plasticity of single dendritic spines. *Nature* **472**, 100-104.
- Nagai, T. and Honda, H.** (2001). A dynamic cell model for the formation of epithelial tissues. *Philos. Mag. B* **81**, 699-719.
- Nandadasa, S., Tao, Q., Menon, N. R., Heasman, J. and Wylie, C.** (2009). N- and E-cadherins in *Xenopus* are specifically required in the neural and non-neural ectoderm, respectively, for F-actin assembly and morphogenetic movements. *Development* **136**, 1327-1338.
- Nieuwkoop, P. D. and Faber, J.** (1967). *Normal Table of Xenopus laevis (Daudin)*. Amsterdam: North-Holland Publ. Co.
- Ohkawara, B., Yamamoto, T. S., Tada, M. and Ueno, N.** (2003). Role of glypican 4 in the regulation of convergent extension movements during gastrulation in *Xenopus laevis*. *Development* **130**, 2129-2138.
- Okuda, S., Inoue, Y., Eiraku, M., Sasai, Y. and Adachi, T.** (2013). Apical contractility in growing epithelium supports robust maintenance of smooth curvatures against cell-division-induced mechanical disturbance. *J. Biomech.* **46**, 1705-1713.
- Rauzi, M., Verant, P., Lecuit, T. and Lenne, P.-F.** (2008). Nature and anisotropy of cortical forces orienting Drosophila tissue morphogenesis. *Nat. Cell Biol.* **10**, 1401-1410.
- Riedl, J., Crevenna, A. H., Kessenbrock, K., Yu, J. H., Neukirchen, D., Bista, M., Bradke, F., Jenne, D., Holak, T. A., Werb, Z. et al.** (2008). Lifeact: a versatile marker to visualize F-actin. *Nat. Methods* **5**, 605-607.
- Sawyer, J. M., Harrell, J. R., Shemer, G., Sullivan-Brown, J., Roh-Johnson, M. and Goldstein, B.** (2010). Apical constriction: a cell shape change that can drive morphogenesis. *Dev. Biol.* **341**, 5-19.
- Schiebert, E. M. and Zsembery, A.** (2003). Extracellular ATP as a signaling molecule for epithelial cells. *Biochim. Biophys. Acta* **1615**, 7-32.
- Shindo, A., Hara, Y., Yamamoto, T. S., Ohkura, M., Nakai, J. and Ueno, N.** (2010). Tissue-tissue interaction-triggered calcium elevation is required for cell polarization during *Xenopus* gastrulation. *PLoS ONE* **5**, e8897.
- Smedley, M. J. and Stanisstreet, M.** (1986). Calcium and neurulation in mammalian embryos. II. Effects of cytoskeletal inhibitors and calcium antagonists on the neural folds of rat embryos. *J. Embryol. Exp. Morphol.* **93**, 167-178.
- Spahn, P. and Reuter, R.** (2013). A vertex model of Drosophila ventral furrow formation. *PLoS ONE* **8**, e75051.
- Suzuki, M., Hara, Y., Takagi, C., Yamamoto, T. S. and Ueno, N.** (2010). MID1 and MID2 are required for *Xenopus* neural tube closure through the regulation of microtubule organization. *Development* **137**, 2329-2339.
- Suzuki, M., Morita, H. and Ueno, N.** (2012). Molecular mechanisms of cell shape changes that contribute to vertebrate neural tube closure. *Dev. Growth Differ.* **54**, 266-276.
- Vicente-Manzanares, M., Ma, X., Adelstein, R. S. and Horwitz, A. R.** (2009). Non-muscle myosin II takes centre stage in cell adhesion and migration. *Nat. Rev. Mol. Cell Biol.* **10**, 778-790.
- Wallingford, J. B. and Harland, R. M.** (2001). *Xenopus* Dishevelled signaling regulates both neural and mesodermal convergent extension: parallel forces elongating the body axis. *Development* **128**, 2581-2592.
- Wallingford, J. B., Ewald, A. J., Harland, R. M. and Fraser, S. E.** (2001). Calcium signaling during convergent extension in *Xenopus*. *Curr. Biol.* **11**, 652-661.
- Xu, S. Z., Zeng, F., Boulay, G., Grimm, C., Harteneck, C. and Beech, D. J.** (2005). Block of TRPC5 channels by 2-aminoethoxydiphenyl borate: a differential, extracellular and voltage-dependent effect. *Br. J. Pharmacol.* **145**, 405-414.
- Zhao, Y., Araki, S., Wu, J., Teramoto, T., Chang, Y.-F., Nakano, M., Abdelfattah, A. S., Fujiwara, M., Ishihara, T., Nagai, T. et al.** (2011). An expanded palette of genetically encoded Ca(2+)(+) indicators. *Science* **333**, 1888-1891.